

Facile production of vitamin B₃ and other heterocyclic carboxylic acids using an efficient Ag/ZnO/graphene-Si hybrid nanocatalyst

Yasser A. Attia^{1,2}  · Carlos Vázquez Vázquez^{1,2} ·
Yasser M. A. Mohamed³

Received: 26 April 2016 / Accepted: 14 June 2016
© Springer Science+Business Media Dordrecht 2016

Abstract High yield of vitamin B₃ is produced using Ag/ZnO/graphene nanocomposite (1 wt%) as a nanocatalyst after its activation by a silicon precursor such as trimethylsilyl chloride (TMSCl) or *tert*-butyldimethylsilyl chloride (TBSCl) under visible light. TBSCl has been proved as more efficient activating agent than TMSCl in the oxidation of heterocyclic alcohol derivatives to afford their corresponding carboxylic acids. 3-Pyridinemethanol was selected to be a model substrate to test the ability of Ag/ZnO/graphene-Si nanocatalysts. The oxidation reaction of alcohols was completed in short reaction time (30–60 min) at ambient condition to yield vitamin B₃ and other heterocyclic carboxylic acids in excellent yields (86–99 %). A catalytic oxidation mechanism that is based on the generation of highly active catalytic oxidation species (oxygen radicals) has been proposed. The utility of this inexpensive and recyclable catalytic system without using molecular oxygen or any oxidants make this procedure interesting from a green chemistry point of view.

✉ Yasser A. Attia
yasserniles@niles.edu.eg

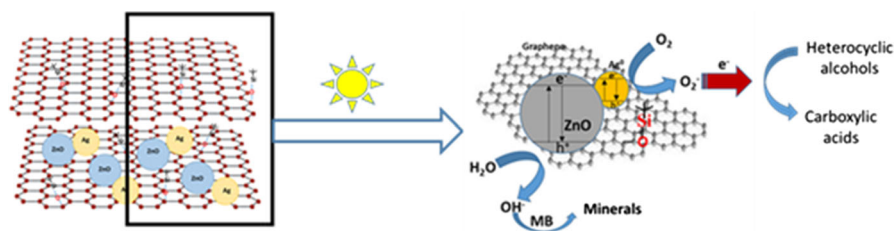
✉ Yasser M. A. Mohamed
y.m.a.mohamed@outlook.com

¹ Department Physical Chemistry, Faculty of Chemistry, Santiago de Compostela University, 15705 Santiago de Compostela, Spain

² National Institute of Laser Enhanced Sciences, Cairo University, Giza 12631, Egypt

³ Photochemistry Department, National Research Center, Dokki, Giza 12622, Egypt

Graphical Abstract



Keywords Heterogeneous nanocatalysts · Ag/ZnO/graphene · Nanocomposite · Catalytic oxidation · Photodegradation · Carboxylic acids and Vitamin B₃

Introduction

Production of nicotinic acid, also known as vitamin B₃, with green procedures has received great attention due to its pharmaceutical use as a vitamin. Every year, an almost 20,000 tons of vitamin B₃ are produced worldwide. Currently, the commonly used oxidizing agent in production of vitamin B₃ is chromic acid, which is characterized as corrosive. In addition, several tons of inorganic waste are produced for every ton of nicotinic acid generated from 3-picoline. Therefore, developing an efficient catalytic system was mandatory to minimize the inorganic wastes and obtain vitamin B₃ in high yield [1]. Production of vitamin B₃ from catalytic oxidation of 3-pyridinemethanol [2], 3-pyridinecarboxyaldehyde [3] or picoline [4] has been reported in several cases, due to its biological importance [5]. These methods have some drawbacks such as selectivity in production of nicotinic acid, long lasting reaction time, the use of high temperature, and the use of expensive materials as catalysts. Nanostructured catalysts are becoming a more popular strategy to provide heterogeneous catalysts with improved characteristics [6–12]. Currently, the use of recyclable nanocatalyst in oxidation reactions has attracted great attention from an eco-friendly point of view [13, 14]. For this purpose, we investigated a recyclable and efficient nanocatalytic system for generating vitamin B₃ in excellent yield, with short reaction time and no waste production.

ZnO/graphene-based nanostructured catalysts are becoming a popular strategy to provide heterogeneous catalysts with improved characteristics, due to broad band-gap energy, cost effectiveness, physicochemical stability, easiness of availability and high oxidative capacity [15–17]. Subsequently, ZnO based nanocomposites have been widely used in different potential applications such as sensors, solar energy conversion devices and photocatalysts [18]. It is worth noticing that although the catalytic behavior of Ag/ZnO/graphene nanocomposite as a photocatalyst for degradation of dyes has been investigated in several reports [16, 17]. However, its catalytic activity towards oxidation of alcohols has not been reported. Graphene-supported noble metal nanoparticles have potential application in catalysis [18]. Furthermore, the adsorption and dissociation of O₂ molecule on pristine and silicon-

doped graphene was investigated by Chen et al. [19]. It has been reported that graphene–silicon interactions exhibited much larger interactions than those normally associated with Wan der Waals forces [20]. In addition, the growth behavior of ZnO in the presence of different concentrations of silicon has been reported by Podbršček et al. [21]. Based on these results, we developed Ag/ZnO/graphene-Si hybrid nanocomposite and exploited it in catalytic oxidation application as a chemical evolution. Hence, due to our continuous interest in the development of heterogeneous catalysts [22, 23], herein we report on the application of Ag/ZnO/graphene nanocomposite mixed with *tert*-butyldimethylsilyl chloride (TBSCl) or trimethylsilyl chloride (TMSCl) to overcome the aforementioned limitation in oxidation processes.

Experimental section

Materials

Graphite powder and potassium permanganate (KMnO₄) were purchased from Alfa Aesar. Sulfuric acid (H₂SO₄), hydrochloric acid (HCl), sodium hydroxide (NaOH), hydrogen peroxide (H₂O₂), ethylene glycol (EG), zinc(II) sulfate, zinc(II) acetate, silver(I) nitrate, *tert*-butyldimethylsilyl chloride (TBSCl), trimethylsilyl chloride (TMSCl), methylene blue dye, methanol, hexane, acetone, Dimethyl Sulfoxide (DMSO), Chloroform, Ethyl acetate (EtOAc), Diethyl ether (Et₂O), 3-Pyridine-methanol, 2-pyridinemethanol, 2-thiophenemethanol and 2-furanmethanol were purchased from Sigma-Aldrich. Deionized water was used in all the experiments.

Characterization

UV–Vis spectra were measured with a Perkin Elmer Lambda 40 UV–visible spectrophotometer using 1-cm path length Hellma quartz cuvettes. Transmission electron microscopy (TEM) images were obtained with a Joel JEM-1230 electron microscope operated at 120 kV equipped with GatanUltraScan 4000SP 4K × 4K CCD camera. A drop from a diluted sample dispersion was deposited onto an amorphous carbon film on 400 mesh copper grids and left to evaporate at room temperature. Scanning electron microscopy (SEM) images were obtained with a ZEISS FE-SEM ULTRA Plus (equipped with EDX analyzer) microscope with a Philips CM20 microscope, operating at an accelerating voltage of 200 kV. Several drops from the sample dispersion were deposited onto an aluminum pin stubs and left to evaporate at room temperature. X-ray diffraction (XRD) measurements were performed using a Philips PW1710 X-ray diffractometer using Cu K α radiation ($\lambda = 1.54186 \text{ \AA}$). The XRD patterns were recorded from 20° to 70°2 Θ with a step size of 0.020°2 Θ and collecting 10 s per step. FT-IR spectra were recorded with a Nicolet 6700 infrared spectrophotometer to determine the specific functional groups present on the surface. Melting points (m.p.) were uncorrected using IA 9100MK-Digital Melting Point Apparatus. Thin layer chromatography (TLC) was done by silica gel plates 60 GF254, cellulose plates (20 × 20 cm). ¹H NMR and ¹³C NMR

spectra were determined on Bruker Avance DPX spectrometer at 300 MHz for ^1H NMR and 75 MHz for ^{13}C NMR. High-resolution mass (ESI-MS) spectra were measured on (TOF) LC/MS; 6230 Series Accurate-Mass Time-of-Flight.

Catalyst preparation

Graphene oxide (GO) was prepared using a modified Hummer's method [24]. In a typical procedure, H_2SO_4 (150 mL) was added into a flask containing graphite (6 g) in an ice bath under stirring. After that, 18 g potassium permanganate (KMnO_4) was slowly added to the above mixture, and the ice bath was removed after several minutes. The color of the solution turned to dark green under continued stirring for 2 h at 35 °C. Then, water (300 mL) was slowly added to the reaction mixture and the conical flask was bathed in boiling water; the reaction mixture was kept at this temperature for another 30 min. After that, the flask was cooled in an ice bath, and 1 L distilled water was added to stop the reaction. 20 mL H_2O_2 (30 %) was added to reduce the residual permanganate to soluble manganese ions. Eventually, the precipitation was centrifuged and washed with 1 M HCl and distilled water several times, and then vacuum dried at 60 °C for 24 h.

To prepare Ag/ZnO/graphene composite via the co-precipitation method, 0.05 g GO dissolved in 40 mL of ethylene glycol (EG) was sonicated for 2 h to give a brown dispersion. To this solution, 0.04 g of zinc acetate and 0.25 g silver nitrate dissolved in 40 mL of EG were added under vigorous stirring, and the stirring was continued for 2 h. Subsequently, 0.025 M NaOH was added to the mixture dropwise followed by stirring for 1 h. Then, the mixture was heated at 160 °C to achieve the reduction of GO and the deposition of ZnO, then washed with ethanol and deionized water five times. Finally, the resultant composite was dried at 70 °C in vacuum for 24 h. The obtained composite (40 mg) was mixed with 10 mg of TBSCl or TMSCl for degradation of methylene blue (MB) dye under low power UV-lamp (Ana-lamp 254 nm) and halogen lamp (HALOPAR 20 75 W 230 V 30° GU10, Italy). The temperature was kept constant at 28 °C all the experiments to avoid the thermal degradation.

Production of vitamin B₃ (nicotinic acid) (2) using Ag/ZnO/graphene-Si catalyst

In a round flask, Ag/ZnO/graphene nanocomposite (10 mg, 1 wt%) was weighted, a mixture of MeOH:H₂O (1:1, 10 mL) was added, and that was followed by addition of *tert*-butyldimethylsilyl chloride (TBSCl) (1.38 g, 9.20 mmol, 1 eq). 3-Pyridine-methanol (**1**) (1.0 g, 9.20 mmol, 1 eq) was subsequently added to the reaction mixture, which was stirred for 30 min at room temperature and monitored by TLC using eluent system (EtOAc:Hexane, 3:7). The mixture was filtrated and then water (5 mL) was added, and the mixture was extracted with (CHCl_3 : MeOH, 1:1) (5 mL \times 2). The collected methanol/water layer was evaporated to afford vitamin B₃ (**2**) in quantitative yield.

Catalyst recovering

The above catalyst was collected on a Buchner funnel and washed with water (30 ml), MeOH (30 ml), acetone (30 ml) and Et₂O (30 ml). The recovered catalyst was then used in another oxidation process of 3-pyridinemethanol (**1**).

*Synthesis of carboxylic acids [pyridine-2-carboxylic acid (**7**), thiophene-2-carboxylic acid (**8**) or furan-2-carboxylic acid (**9**)*

An appropriate alcohol [2-pyridinemethanol (**3**) (1.0 g, 9.20 mmol, 1 eq), 2-thiophenemethanol (**4**) (1.0 g, 8.78 mmol, 1 eq) or 2-furanmethanol (**5**) (1.0 g, 10.20 mmol)] was added to reaction mixture that contained Ag/ZnO/graphene nanocomposite (10 mg, 1 wt%), and TBSCl (1.38 g, 9.20 mmol, 1 eq), (1.32 g, 8.78 mmol, 1 eq), (1.53 g, 10.20 mmol, 1 eq) or (1.38 g, 9.26 mmol, 1 eq) dissolved in MeOH:H₂O (1:1, 10 mL). The mixture was stirred for 30, 60 or 60 min, respectively, at room temperature and monitored by TLC using eluent system (EtOAc:Hexane, 3:7). The mixture was filtrated and then water (5 mL) was added, and the mixture was extracted with (CHCl₃: MeOH, 1:1) (5 mL × 2). The collected methanol/water layer was evaporated using rotary evaporator to afford the residue that was purified by column chromatography using silica gel (Hexane:EtOAc, 7:3, 6:4 and then 1:1) to afford the corresponding carboxylic acids; pyridine-2-carboxylic acid (**7**); thiophene-2-carboxylic acid (**8**) or furan-2-carboxylic acid (**9**) respectively.

The spectroscopic data of the products are shown as following:

Nicotinic acid (2) Yield (0.99 g, 99 %), ¹H NMR (300 MHz, DMSO-*d*₆): δ (ppm) 12.09 (br, s, 1H), 9.14 (dd, *J* = 2.1, 0.6 Hz, 1H), 8.79 (*d*, 1.7 Hz, 1H), 8.27 (dt, 7.4, 2.0 Hz, 1H), 7.52 (dd, 7.4, 4.9 Hz, 1H); ¹³C NMR (75 MHz, DMSO-*d*₆): δ (ppm) 166.5, 153.8, 150.1, 136.09, 126.4, 124.1; HRMS (ESI): *m/z* calcd for C₆H₅O₂N: 123.0320, found: 122.0316 [M-1]⁺.

Pyridine-2-carboxylic acid (7) Yield (0.97 g, 97 %), m.p. 136–137 °C, ¹H NMR (300 MHz, DMSO-*d*₆): δ (ppm) 12.13 (br, s, 1H), 8.68 (dd, *J* = 4.6, 1.6 Hz, 1H), 8.04 (dt, *J* = 7.6, 1.0 Hz, 1H), 7.91 (dt, *J* = 4.0, 1.3 Hz, 1H), 7.58 (dd, *J* = 7.6, 4.0 Hz, 1H); ¹³C NMR (75 MHz, DMSO-*d*₆): δ (ppm) 166.2, 149.0, 137.8, 148.7, 127.9, 125.0. HRMS (ESI): *m/z* calcd for C₆H₅O₂N: 123.0320, found: 122.0311[M-1]⁺.

Thiophene-2-carboxylic acid (8) Yield (0.92, 92 %), m.p. 129–130 °C. ¹H NMR (300 MHz, DMSO-*d*₆): δ (ppm) 12.09 (br, s, 1H), 7.88 (dd, *J* = 4.8, 1.2 Hz, 1H), 7.72 (dd, *J* = 3.6, 1.2 Hz, 1H), 7.21 (dd, *J* = 4.8, 3.7 Hz, 1H). ¹³C NMR (75 MHz, DMSO-*d*₆): δ (ppm) 162.5, 134.1, 133.9, 132.9, 128.7. HRMS (ESI): *m/z* calcd for C₅H₄O₂S: 127.9932, found: 126.9927 [M-1]⁺.

Furan-2-carboxylic acid (9) Yield (0.86, 86 %), m.p. 132–34 °C; ^1H NMR (300 MHz, DMSO- d^6): δ (ppm) 12.08 (br, s, 1H), 7.94 (dd, $J = 3.6$, 1.2 Hz, 1H), 7.21 (dd, $J = 3.6$, 1.2 Hz, 1H), 6.65 (dd, $J = 1.2$, 2.8 Hz, 1H); ^{13}C NMR (75 MHz, DMSO- d^6): δ (ppm) 159.8, 146.8, 144.3, 117.9, 112.6. HRMS (ESI): m/z calcd for $\text{C}_5\text{H}_4\text{O}_3$: 112.0160, found: 111.0157 $[\text{M}-1]^+$.

Results and discussion

Through the co-precipitation synthesis process, reduction of graphene oxide and loading of Ag nanoparticles and ZnO nanoparticles on two-dimensional graphene sheets were achieved to form the visible photoresponsive Ag/ZnO/Graphene nanocomposites for the photodegradation of organic dyes. The TEM and SEM images of the obtained products are depicted in Fig. 1. The TEM image shows that the as-prepared ZnO NPs has a uniform diameter of $\sim 86.4 \pm 1.8$ nm (Fig. 1a). Figure 1b shows the loading of ZnO on graphene sheets. An important decrease in the particle size of ZnO nanoparticles is observed (36.1 ± 1.4 nm). This change is related to the presence of polar groups ($-\text{OH}$, $-\text{C}(\text{O})\text{OH}$, $-\text{C}(\text{O})-$, $-\text{O}-$) in the starting graphene oxide material, that act as nucleation sites for the formation of ZnO nanoparticles and favor the control of the ZnO growth. Ag/ZnO NPs are homogeneously dispersed and anchored on the graphene sheets, as shown in TEM image (Fig. 1c). The larger nanoparticles (~ 10 – 50 nm) correspond mainly to Ag NPs due to their larger electron contrast and also to the larger molar content in the Ag/ZnO/Graphene nanocomposite synthesis; on the other hand, ZnO NPs are very small with an average particle size of 1.9 ± 0.5 nm. The SEM image of GO indicates the product has two-dimensional sheets structure (Fig. 1d). It could be further confirmed by the corresponding SEM image of the composite (Fig. 1e, f), considering the oxygen containing groups such as carboxyl in GO serve as anchoring sites to direct coating process, that the Ag/ZnO NPs were homogeneously formed on the graphene sheets and free from aggregation. The chemical composition of Ag/ZnO/graphene was analyzed by an energy dispersive spectrometer (EDS) spectrum via SEM (Fig. 1g) and elemental mapping (Fig. 1h–k). The results show the peaks of C, O, Zn and Ag, confirming the sample is of high purity.

The absorbance spectra of the prepared samples are shown in Fig. 2. ZnO nanoparticles showed a maximum absorbance at 298 nm that shifted to longer wavelength with loading on graphene sheets to 348 nm, and with the addition of Ag nanoparticles, shifted to 307 nm in addition to the plasmonic band of silver nanoparticles that appears at 398 nm. In Ag/ZnO/graphene, two peaks are shown at 318 and 402 nm, corresponding to ZnO and Ag nanoparticles respectively.

The prepared Ag/ZnO/graphene nanocomposites mainly show diffraction peaks as in Fig. 3, located at 38.23° , 44.42° , and 64.60° 2θ , corresponding to the presence of Ag (0) nanoparticles. Very low intensity peaks are observed in the angle range where ZnO is observed, indicating probably very small particle sizes, low crystallinity or low content. No evidence of initially formed Ag_2O is observed after the aging step at 150 °C, although it readily forms after addition of NaOH to Ag (I) solutions. The broad band at 20° – 25° 2θ is related to rGO. By introducing Si

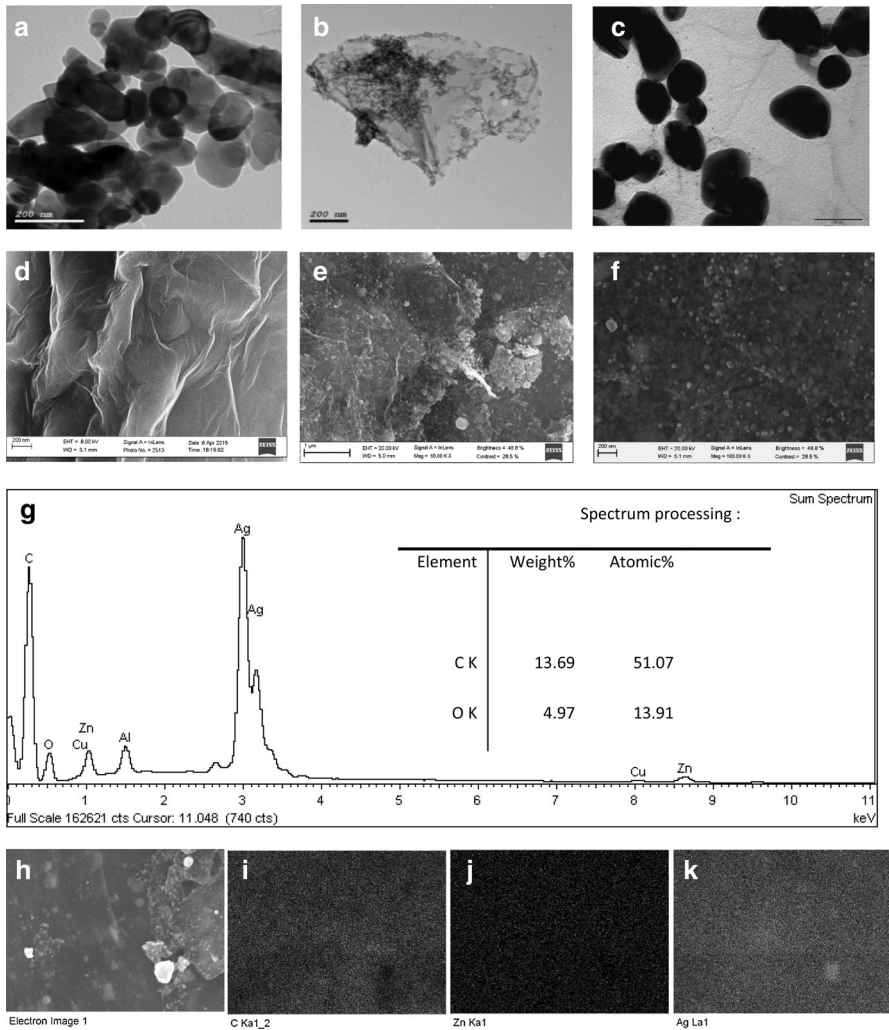


Fig. 1 **a** TEM images of ZnO NPs, **b** ZnO/graphene nanocomposites, and **c** Ag/ZnO/graphene nanocomposites respectively. **d** SEM images of graphene oxide, **e** Ag/ZnO/graphene nanocomposites, and **f** Ag/ZnO/graphene-Si nanocomposites respectively. **g** EDS analysis of Ag/ZnO/graphene nanocomposites, and **h–k** elemental mapping

from TBSCl or TMSCl to Ag/ZnO/graphene composites, other peaks located at 70.93°, 69.86°, 58.59°, 49.64°, 36.21° and 33.74° 2θ corresponding to Si are observed.

Photocatalytic activity towards degradation of methylene blue (MB) dye

The photocatalytic performance of the samples (Ag/ZnO/graphene and Ag/ZnO/graphene-Si) was monitored by degradation of methylene blue dye (MB) in

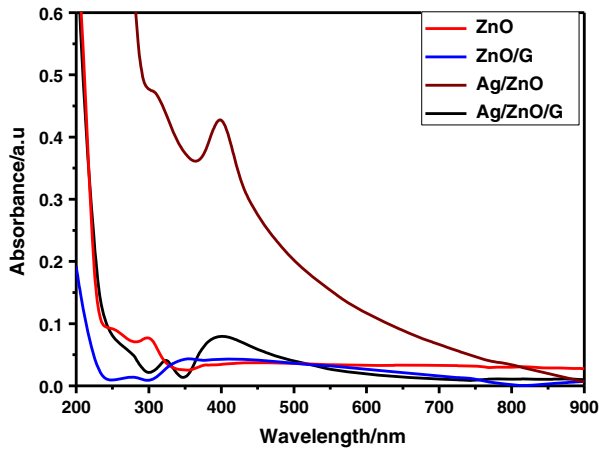


Fig. 2 Absorption spectra of ZnO, ZnO/graphene, Ag/ZnO, and Ag/ZnO/graphene

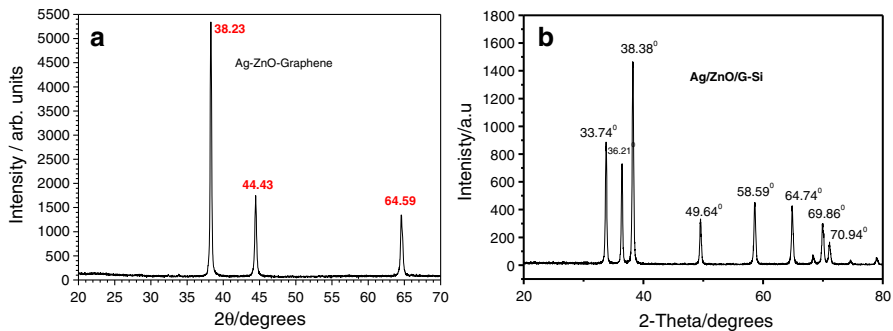
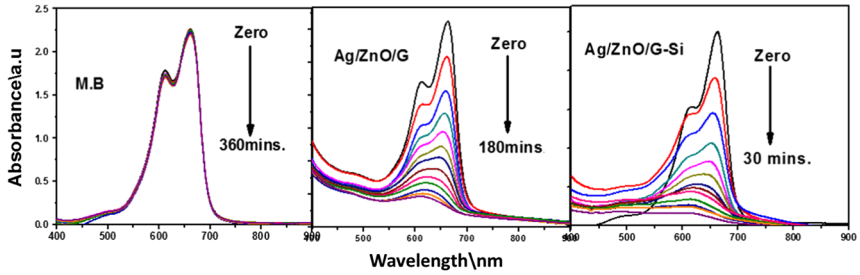


Fig. 3 **a** The XRD patterns of Ag/ZnO/graphene composite, and **b** Ag/ZnO/G-Si composite

aqueous solution under low power UV and visible irradiation. The photodegradation was followed by measuring UV–visible absorption spectra at different irradiation times (Fig. 4).

As shown in Fig. 4, MB dye is photodegraded within 60 min with Ag/ZnO/graphene photocatalyst under UV-light. However, only 10 min was enough for complete degradation of MB with Ag/ZnO/graphene-Si as a new nanocatalyst. However, under visible light, we can observe that loading of Ag/ZnO on graphene sheets enhanced the photocatalytic activity for MB dye degradation, but with longer irradiation time of 180 min, and only 30 min was enough for complete degradation of MB under visible light with Ag/ZnO/graphene-Si composites. The photodegradation rate order under UV and visible light irradiation of the samples is: Ag/ZnO/graphene-Si > Ag/ZnO/graphene. These results indicate that the photocatalytic performance can be enhanced by incorporation Ag/ZnO on graphene sheets and it becomes highly effective by introducing Si to Ag/ZnO/graphene composite. The enhanced photocatalytic performance suggests that the ternary composite (Ag/

Visible



UV

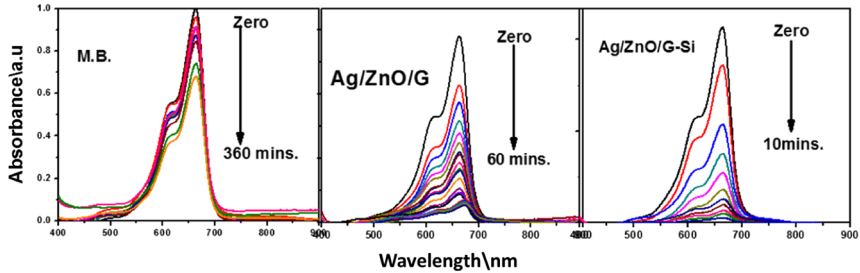


Fig. 4 Absorption spectra showing the MB dye photodegradation using Ag/ZnO/graphene and Ag/ZnO/graphene-Si composites under UV and visible irradiation

ZnO/graphene-Si) can be served as highly efficient photocatalyst for degradation of organics in aquatic environmental.

The mechanisms of photodegradation of MB by Ag/ZnO/graphene under UV and visible light have been proposed [16, 17, 25–29]. It can be summarized as follows: when the photoreaction vessel (MB solution with Ag/ZnO/graphene powder) is irradiated under UV/visible light, photoinduced electrons and holes are formed due to the excitation of ZnO. Then, radicals can capture the electrons or holes, the organic compounds will be degraded [29]. However, from our results, Si from TBSCl or TMSCl further enhanced the photocatalytic activities of the doped Ag/ZnO/graphene samples, because it effectively improves the charge separation efficiency. In Ag/ZnO/graphene-Si composites, photoinduced electron due to excitation of ZnO by visible light with narrow band gap of Ag/ZnO (3.24 to 3.03 eV) [16] can be transferred to graphene, silver NPs, Si and to the model organic dye. Finally, the electrons generated react with dissolved oxygen molecules, producing oxygen peroxide radicals. The hole can react with the hydroxide ion from water to form hydroxyl radicals. These generated radicals from Ag/ZnO/graphene-Si composite can cause the oxidative decomposition of dyes like MB [28]. Also, when we start with graphene oxide and produce reduced GO, there are still some –OH and –COOH groups in the graphene; in particular, more in the edges. Cl[–] can be easily removed from TBSCl or TMSCl by these –OH groups forming C–O–Si bonds, as shown in FT-IR spectra of reduced graphene oxide, Ag/Zn/graphene and Ag/ZnO/graphene-Si composites (Fig. 5). The –OH group that appears in the Fourier transform infrared spectroscopy (FT-IR) spectrum of Ag/ZnO/G at

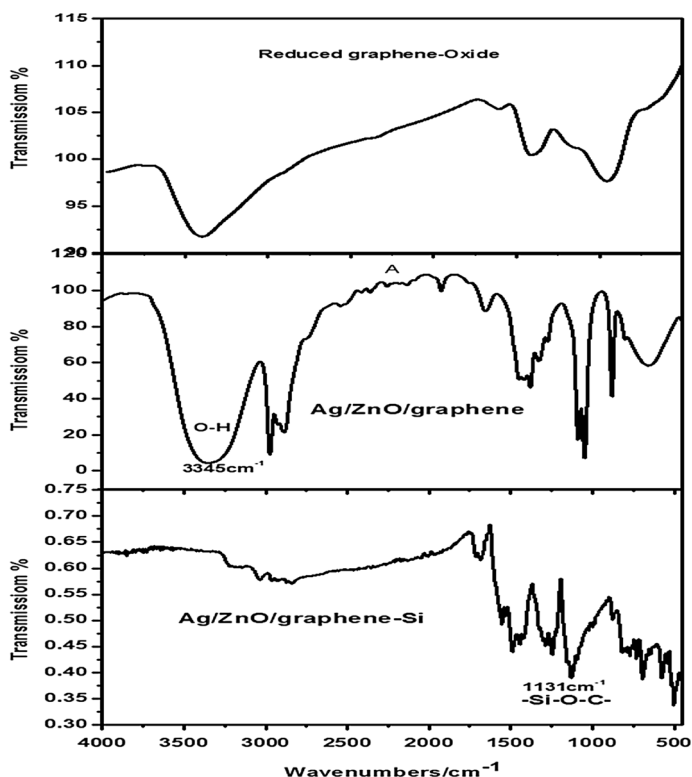
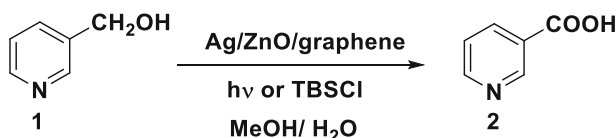


Fig. 5 FT-IR of reduced graphene oxide, Ag/ZnO/graphene and Ag/ZnO/graphene-Si hybrid nanocomposites

3345 cm^{-1} disappeared in Ag/ZnO/G-Si and another band was observed at 1131 cm^{-1} corresponding to $-\text{Si}-\text{O}-\text{C}-$ bond. Moreover, it is reported that TBSCl or TMSCl are common protecting reagents for acids and alcohols [30–32]. This protecting ability seems to make the rGO sheets more hydrophobic due to the alkyl chains, but maybe it favors the adsorption of aromatic molecules on the rGO sheets, explaining the increased efficiency.

Catalytic oxidation activity towards organic substrates: novel commercially production method for vitamin B₃

It is noteworthy that the Ag/ZnO/graphene catalyst has not been reported in the oxidation of organic substrates. Our initial attempts are to optimize the reaction conditions using 3-pyridinemethanol (**1**) as the model substrate (Scheme 1). When Ag/ZnO/graphene (1 wt%) was employed for oxidation reaction of 3-pyridinemethanol (**1**) at room temperature after 24 h, the starting material was recovered and there was no conversion of alcohol **1** (entry 1, Table 1). Since our aim is to develop affordable and relatively accessible methodology, performing the catalytic



Scheme 1 Catalytic oxidation of 3-pyridinemethanol (**1**) to nicotinic acid **2** (vitamin B₃)

Table 1 The concentration of TBSCl that mixing with Ag/ZnO/graphene versus the yield of nicotinic acid (**2**)

Entry	Catalyst ^a	Additives	Time of reaction	Yield ^b (%)
1	Ag/ZnO/graphene	In dark	24 h	–
2	Ag/ZnO/graphene	hv (360–700 nm)	24 h	20
3	Ag/ZnO/graphene	TBSCl (1 mol%)	24 h	5
4	Ag/ZnO/graphene	TBSCl (10 mol%)	24 h	12
5	Ag/ZnO/graphene	TBSCl (0.25 eq.)	24 h	40
6	Ag/ZnO/graphene	TBSCl (0.5 eq.)	24 h	70
7	Ag/ZnO/graphene	TBSCl (1 eq.)	30 min	99

^a Ag/ZnO/graphene (1 wt%)

^b Isolated yield

oxidation reaction using visible light was developed. The reaction mixture that consisted of 3-pyridinemethanol (**1**) and the catalyst (1 wt%) in methanol/water was irradiated using a halogen lamp in the visible region (360–700 nm), but disappointing yield (20 %) of nicotinic acid (**2**) after 24 h was observed (entry 2, Table 1). Hence, we started to study the influence of adding different concentrations of TBSCl as a precursor of a silicon substrate on the Ag/ZnO/graphene nanocomposite catalyst (1 wt%) under normal conditions. In the absence of the catalyst, TMSCl or TBSCl was initially added to a solution of 3-pyridinemethanol (**1**) dissolved in a mixture of methanol/water with stirring at room temperature for 24 h, and no reaction was observed. When one equivalent of TBSCl was added to the Ag/ZnO/graphene nanocomposite catalyst (1 wt%), 5 % isolated yield of nicotinic acid (**2**) was produced (entry 3, Table 1). By increasing the amount of TBSCl using 10 mol%, acid **2** was obtained with 12 % isolated yield (entry 4, Table 1). However, adding 0.25 equivalent of TBSCl produced acid **2** in 40 % isolated yield (entry 5, Table 1) after chromatographic purification. An improved catalytic activity of the catalyst was observed by adding 0.5 equivalents of TBSCl. The acid (**2**) was formed in 70 % isolated yield (entry 6, Table 1). Pleasingly, addition of one equivalent of TBSCl resulted in full conversion of alcohol (**1**) to afford the corresponding acid (**2**) in 99 % isolated yield after 30 min at room temperature (entry 7, Table 1). However, when one equivalent of trimethylsilyl chloride (TMSCl) was used for activation of Ag/ZnO/graphene nanocomposite in the catalytic oxidation reaction of alcohol (**1**), nicotinic acid (**2**) was only obtained in 74 % isolated yield. That might be because the TBS ether could be formed during the oxidation reaction, which had been proven earlier to be more stable than TMS ether (ca. $\sim 10^4$ times) [33]. In addition, other

studies confirmed our investigation by using TBS ether in selective oxidation processes in combination with $\text{Bi}(\text{OTf})_3$ [34] and with CrO_3 [35]. The catalytic activity of graphene oxide (GO) or reduced graphene oxide (r-GO) was examined at oxidation of 3-pyridinemethanol, but the starting material was recovered. Again, when graphene oxide mixed with TBSCl, the alcohol (**1**) was recovered. However, when graphene (G) was mixed with TBSCl, nicotinic acid (**2**) was formed in trace amount with 10 % isolated yield after 24 h. Therefore, we concluded that the most efficient catalytic system was Ag/ZnO/graphene-Si system.

Recyclability of the catalyst was tested for five cycles (see Table 2).

The first recycled catalyst (1 wt%) with one equivalent of TBSCl was employed in oxidation of 3-pyridinemethanol (**1**) to afford acid (**2**) in 99 % isolated yield. Nicotinic acid (**2**) was yielded in 98 % isolated yield in the second recycled batch. However, in the third recycled batch, acid (**2**) was afforded in 98 % isolated yield. The fourth and fifth recycled catalyst was employed in oxidation reaction to produce 97 and 95 % isolated yield. These results emphasize the ability to reuse the developed catalytic oxidation system in this report for a great number of cycles, producing excellent yield in each recycle.

In order to show the merit of Ag/ZnO/G-Si hybrid nanocomposite with recently reported protocols, some homogeneous and heterogeneous catalysts in the oxidation of 3-pyridinemethanol (3-PM) and 3-picoline to afford vitamin B₃ are presented in Table 3.

From the results in Tables 2 and 3, we can say that the loading of Si on the Ag/ZnO/graphene nanocomposite enhanced the oxidation formation of vitamin B₃ from 3-pyridinemethanol (**1**). This procedure can be considered as a new production method for vitamin B₃ with an excellent yield (99 %) in a short reaction time. Moreover, the catalyst is recyclable and reusable in further oxidation reactions.

Other heterocyclic alcohols were employed as substrates (scheme 2). 2-Pyridinemethanol (**3**), 2-thiophenemethanol (**4**) and 2-furanmethanol (**5**) were oxidized using Ag/ZnO/graphene nanocomposite catalyst (1 wt%) with one equivalent of TBSCl to produce pyridine-2-carboxylic acid (**7**), thiophene-2-carboxylic acid (**8**) and furan-2-carboxylic acid (**9**) in 97, 92, and 86 % isolated yield, respectively, after chromatographic purification (Table 4). The ¹H NMR for compound **2** revealed a broad peak at $\delta = 12.09$ ppm, which characterized for carboxylic acid group. In addition, the ¹³C NMR showed a characteristic peak for (COOH) group at 166.5 ppm. The spectroscopic data for all prepared compounds were in accordance with the assigned structures [36–38].

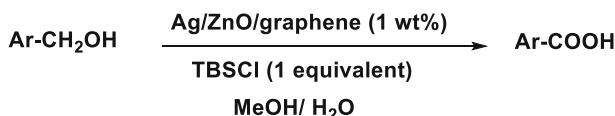
Table 2 Recyclability of the used catalyst in the oxidative reaction of 3-pyridinemethanol (**1**) to nicotinic acid (**2**) (vitamin B₃)

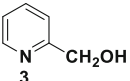
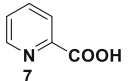
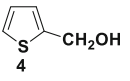
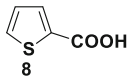
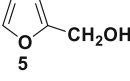
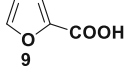
Entry	Recycling	Time of reaction (min)	Yield (%)
1	1st	30	99
2	2nd	30	98
3	3rd	30	98
4	4th	30	97
5	5th	30	95

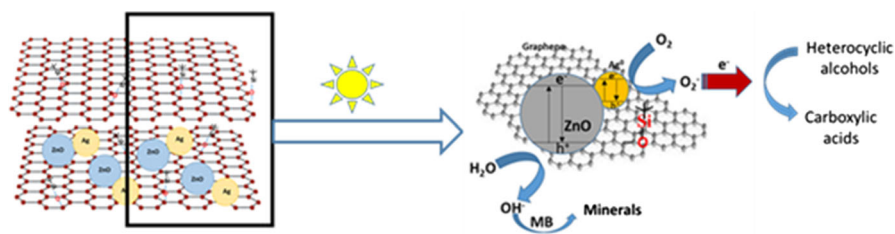
Table 3 Comparison of the catalytic efficiency of Ag/ZnO/G-Si hybrid nanocomposite against other catalysts used for obtaining vitamin B₃ reported in literature

Catalyst	Oxidant	RX condition	Substrate	Time	Conversion (%)	Selectivity (%)	References
Mn ^{III} AlPO-5	APB ^a	75 °C	3- Picoline	4 h	37	78	[1]
CuSO ₄ and TiO ₂ /graphene-like	ND ^b	UV/solar simulated radiation/room temperature	3-PM	5 h	63	34	[2]
Sacrificial TiO ₂	ND ^b	Solar simulated radiation/15–35 °C	3-PM	3 h	25	29	[3]
Iridium–Bismuth cluster complexes	APB ^a	65 °C	3- Picoline	45 min	29	90	[4]
Ag/ZnO/graphene-Si hybrid nanocomposite	ND ^b	Ambient condition	3-PM	30 min	>99 ^c	99 ^d	This report

^a APB acetyl peroxyborate^b ND without oxidant^c Determined by LC/MS analysis^d Isolated yield

**Scheme 2** Catalytic oxidation of alcohol derivatives (3–5) to the corresponding carboxylic acids (7–9)**Table 4** Catalytic oxidation of heterocyclic alcohols to corresponding carboxylic acids

Substrates	Products	Reaction time (min)	Yield (%) ^a
		30	97
		60	92
		60	86

^a Isolated yield after chromatographic purification**Scheme 3** Catalytic oxidation mechanism by Ag/ZnO/graphene-Si hybrid system

Hence, adding Si activates Ag/ZnO/graphene nanocomposite and then promotes the spilling of oxygen over the surface of the catalyst under visible light due to the formation of Ag/ZnO/graphene-Si hybrid catalyst. The contrasting catalytic behaviors afforded by the Ag/ZnO/graphene nanocomposite catalyst with Si could be represented in Scheme 3.

Conclusions

Herein, we report a green procedure for oxidation of 3-pyridinemethanol and other heterocyclic alcohols using Ag/ZnO/graphene-Si nanocatalytic system without using molecular oxygen or any source of oxidants. The catalyst selectively attacks the hydroxyl group in the primary alcohol group in 3-pyridinemethanol without affecting on the nitrogen group in pyridine ring to produce nicotinic acid (vitamin

B₃) in quantitative yield. In order to generalize the oxidation procedure, other heterocyclic alcohols such as 2-pyridinemethanol, 2-thiophenemethanol and 2-furanmethanol acid were subjected to the oxidation reaction condition to afford their corresponding carboxylic acid derivatives in excellent yields. The hydroxyl ions generated in situ due to presence of electrons and holes at the surface of the catalyst (Ag/ZnO/graphene) after activation by TBSCl or TMSCl provide fast reaction with selectivity. Herein, we investigated the catalytic property of Ag/ZnO/graphene in oxidation of organic compounds to produce pharmaceutical products with a simple procedure, which could be considered to be an environmentally benign method. The new oxidation methodology is characterized by its simplicity, ease to work up, works efficiency without adding oxidative species, and eco-friendliness, and could be applied industrially.

Acknowledgments This work was supported by MINECO, Spain (MAT2012-36754-C02-01 and MAT2015- 67458-P), Xunta de Galicia, Spain (GRC2013-044, FEDER Funds).

References

1. R. Raja, J.M. Thomas, M. Greenhill-Hooper, S.V. Ley, F.A.A. Paz, *Facile*. *Chem. Eur. J.* **14**, 2340–2348 (2008)
2. M. Alfè, D. Spasiano, V. Gargiulo, G. Vitiello, R. Di Capua, R. Marotta, *Appl. Catal. A* **487**, 91–99 (2014)
3. D. Spasiano, R. Marotta, I.D. Somma, G. Mancini, *Appl. Catal. B Environ.* **163**, 248–257 (2015)
4. R.D. Adams, M. Chen, G. Elpitiya, M.E. Potter, R. Raja, *ACS Catal.* **3**(12), 3106–3110 (2013)
5. J.K. Duggal, M. Singh, N. Attri, P.P. Singh, N. Ahmed, S. Pahwa, J. Molnar, S. Singh, S. Khosla, R. Arora, *J. Cardiovasc. Pharmacol. Ther.* **15**(2), 158–166 (2010)
6. V. Polshettiwar, R. Luque, A. Fihri, H. Zhu, M. Bouhrara, J.-M. Basset, *Chem. Rev.* **111**, 3036–3075 (2011)
7. A. Maleki, *RSC Adv.* **4**, 64169–64173 (2014)
8. A. Maleki, *Tetrahedron* **68**, 7827–7833 (2012)
9. Q. Li, X. Qina, Y. Luoa, W. Lua, G. Changa, A.M. Asiri, A.O. Al-Youbib, X. Sun, *Electrochim. Acta* **83**, 283–287 (2012)
10. S. Liu, J. Tian, L. Wang, H. Li, Y. Zhang, X. Sun, *Macromolecules* **43**, 10078–10083 (2010)
11. J. Tian, S. Liu, Y. Zhang, H. Li, L. Wang, Y. Luo, A.M. Asiri, A.O. Al-Youbi, X. Sun, *Inorg. Chem.* **51**, 4742–4746 (2012)
12. H. Moussa, E. Giro, K. Mozet, H. Alem, G. Medjahdi, R. Schneider, *Appl. Catal. B Environ.* **185**, 11–21 (2016)
13. J. Tian, S. Liu, H. Li, L. Wang, Y. Zhang, Y. Luo, A.M. Asiri, A.O. Al-Youbi, X. Sun, *RSC Adv.* **2**, 1318–1321 (2012)
14. M.B. Gawande, A.K. Rathi, J. Tucek, K. Safarova, N. Bundaleski, O.M.N.D. Teodoro, L. Kvitek, R.S. Varma, R. Zboril, *Green Chem.* **16**, 4137–4143 (2014)
15. C.W. Lim, I.S. Lee, *Nano Today* **5**, 412–434 (2010)
16. M. Ahmad, E. Ahmed, Z.L. Hong, N.R. Khalid, W. Ahmed, A. Elhissi, *J. Alloy. Compd.* **577**, 717–727 (2013)
17. M. Ahmad, E. Ahmed, Z.L. Hong, J.F. Xu, N.R. Khalid, A. Elhissi, W. Ahmed, *Appl. Surf. Sci.* **274**, 273–281 (2013)
18. P.V. Kamat, *J. Phys. Chem. Lett.* **1**(2), 520–527 (2010)
19. Y. Chen, X.C. Yang, Y.J. Liu, J.X. Zhao, Q.H. Cai, X.Z. Wang, *J. Mol. Graph. Model.* **39**, 126–132 (2013)
20. S.R. Na, J.W. Suk, R.S. Ruoff, R. Huang, K.M. Liechti, *ACS Nano* **8**(11), 11234–11242 (2014)
21. P. Podbršček, G. Dražić, J.A. Paramo, Y.M. Strzhemechny, J. Maček, Z.C. Orel, *CrystEngComm* **12**, 3071–3079 (2010)

22. Y. Attia, D. Buceta, C. Blanco-Varela, M. Mohamed, G. Barone, M.A. López-Quintela, *J. Am. Chem. Soc.* **136**, 1182–1185 (2014)
23. Y.M. Mohamed, T.V. Hansen, *Tetrahedron* **69**(19), 3872–3877 (2013)
24. W.S. Hummers, R.E. Offeman, *J. Am. Chem. Soc.* **80**(1937), 1339 (1958)
25. S.S. Kumar, P. Venkateswarlu, V.R. Rao, G.N. Rao, *Int. Nano Lett.* **3**(30), 1–6 (2013)
26. S. Pyne, G.P. Sahoo, D.K. Bhui, H. Bar, P. Sarkar, S. Samanta, A. Maity, A. Misra, *Spectrochim. Acta Part A Mol. Biomol. Spectrosc.* **93**, 100–105 (2012)
27. F. Xu, Y. Yuan, D. Wu, M. Zhao, Z. Gao, K. Jiang, *Mater. Res. Bull.* **48**, 2066–2070 (2013)
28. X. Liu, L. Pan, Q. Zhao, G. Zhu, T. Lv, G. Zhu, T. Chen, T. Lu, Z. Sun, C. Sun, *Chem. Eng. J.* **183**, 238–243 (2012)
29. Z. Xiong, L.L. Zhang, J.Z. Ma, X.S. Zhao, *Chem. Commun.* **46**, 6099–6101 (2010)
30. E.J. Corey, *J. Am. Chem. Soc.* **94**, 6190–6191 (1972)
31. A. Bartoszewicz, M. Kalek, J. Nilsson, R. Hiresova, J. Stawinski, *Synlett* (2008). doi:[10.1055/s-2007-992379](https://doi.org/10.1055/s-2007-992379)
32. L.H. Finger, B. Scheibe, J. Sundermeyer, *Inorg. Chem.* **54**(19), 9568–9575 (2015)
33. Y. Kita, N. Shibata, T. Tohjo, N. Yoshida, *J. Chem. Soc., Perkin Trans. 1* (1992). doi:[10.1039/P19920001795](https://doi.org/10.1039/P19920001795)
34. B. Barnych, J.M. Vatèle, *Synlett* **14**(11), 2048–2052 (2011)
35. S. Zhang, L. Xu, M.L. Trudell, *Synthesis* **11**, 1757–1760 (2005)
36. L. Zhou, M. Chen, Y. Wang, Y. Su, X. Yang, *Appl. Catal. A* **475**, 347–354 (2014)
37. B. Bechi, S. Herter, S. McKenna, C. Riley, S. Leimkühler, N.J. Turner, A.J. Carnell, *Green Chem.* **16**(10), 4524–4529 (2014)
38. R. Zheng, Q. Zhou, H. Gu, H. Jiang, J. Wu, Z. Jin, D. Han, G. Dai, R. Chen, *Tetrahedron Lett.* **55**(41), 5671–5675 (2014)